Synergic Deep Learning for Smart Health Diagnosis of COVID-19 for Connected Living and Smart Cities

K. SHANKAR and ESWARAN PERUMAL, Department of Computer Applications, Alagappa University, India
MOHAMED ELHOSENY, College of Computer Information Technology, American University in the Emirates, UAE
FATMA TAHER, Department of Computing and Applied Technology, Zayed University, UAE
B. B. GUPTA, Computer Engineering Department, NIT Kurukshetra, India and Department of Computer Science and Information Engineering, Asia University, Taiwan
AHMED A. ABD EL-LATIF, Mathematics and Computer Science Department, Faculty of Science, Menoufia University, Egypt

COVID-19 pandemic has led to a significant loss of global deaths, economical status, and so on. To prevent and control COVID-19, a range of smart, complex, spatially heterogeneous, control solutions, and strategies have been conducted. Earlier classification of 2019 novel coronavirus disease (COVID-19) is needed to cure and control the disease. It results in a requirement of secondary diagnosis models, since no precise automated toolkits exist. The latest finding attained using radiological imaging techniques highlighted that the images hold noticeable details regarding the COVID-19 virus. The application of recent artificial intelligence (AI) and deep learning (DL) approaches integrated to radiological images finds useful to accurately detect the disease. This article introduces a new synergic deep learning (SDL)-based smart health diagnosis of COVID-19 using Chest X-Ray Images. The SDL makes use of dual deep convolutional neural networks (DCNNs) and involves a mutual learning process from one another. Particularly, the representation of images learned by both DCNNs is provided as the input of a synergic network, which has a fully connected structure and predicts whether the pair of input images come under the identical class. Besides, the proposed SDL model involves a fuzzy bilateral filtering (FBF) model to pre-process the input image. The integration of FBL and SDL resulted in the effective classification of COVID-19. To investigate the classifier outcome of the SDL model, a detailed set of simulations takes place and ensures the effective performance of the FBF-SDL model over the compared methods.

Authors' addresses: K. Shankar and E. Perumal, Department of Computer Applications, Alagappa University, Karaikudi, Tamil Nadu, 630003, India; emails: drkshankar@ieee.org, eswaran@alagappauniversity.ac.in; M. Elhoseny, College of Computer Information Technology, American University in the Emirates, Dubai, Dubai International Academic City, P.O. Box: 503000, Dubai, UAE; email: mohamed.elhoseny@aue.ae; F. Taher, Department of Computing and Applied Technology, Zayed University, Dubai, Academic City, UAE; email: Fatma.taher@zu.ac.ae; B. B. Gupta, Department of Computer Engineering, National Institute of Technology Kurukshetra, Kurukshetra, 136119, Haryana, India; Department of Computer Science and Information Engineering, Asia University, Taichung, Taiwan; Staffordshire University, University House Leek Road, Stoke-on-Trent, ST4 2DF, UK; email: Gupta.brij@gmail.com; A. A. Abd El-Latif, Mathematics and Computer Science Department, Faculty of Science, Menoufia University, Shebin El-Koom, 32511, Egypt; emails: a.rahiem@gmail.com, alatif@science.menofia.edu.eg.

1533-5399/2021/11-ART61 $15.00
https://doi.org/10.1145/3453168

CCS Concepts: • **Information systems → Information systems applications;**

Additional Key Words and Phrases: COVID-19, classification, deep neural network, deep learning, pre-processing

ACM Reference format:
K. Shankar, Eswaran Perumal, Mohamed Elhoseny, Fatma Taher, B. B. Gupta, and Ahmed A. Abd El-Latif. 2021. Synergic Deep Learning for Smart Health Diagnosis of COVID-19 for Connected Living and Smart Cities. *ACM Trans. Internet Technol.* 22, 3, Article 61 (November 2021), 14 pages.
https://doi.org/10.1145/3453168

1 INTRODUCTION

At present times, smart healthcare for disease diagnosis and prevention concentrates on the advancement in healthcare technology for improving human health at every level by the use of smart technologies. Due to the improvements in information technologies, the idea of smart healthcare has progressively come to the fore [2, 13]. It makes use of the latest developments such as **internet of things (IoT)**, cloud computing, and artificial intelligence, for transforming the classical medical system in an all-round way, making healthcare more efficient, more convenient, and more personalized. Owing to the introduction of smart healthcare, the detection of COVID-19 becomes essential. COVID-19 is considered as an epidemic infection [1, 16, 17, 24, 30]. It is called COVID-19, which belongs to the family of SARS-CoV-2. Initially, it was discovered from Wuhan and started rapidly spreading over China. Then, in the USA, around 7 cases were assumed as positive for corona on January 20, 2020, which has reached the number of 300,000 by 5 April, 2020. The major source of coronaviruses was animals; however, it spreads over human beings due to zoonotic behavior. **Severe acute respiratory syndrome Coronavirus (SARS-CoV)** as well as **Middle East respiratory syndrome Coronavirus (MERS-CoV)** are seemed as the major reason for respiratory infections and results in mortality [18]. The general signs of COVID-19 are severe fever, dry cough, headache, fatigue, muscle cramps, breathing problems, and so on. To predict the COVID-19, **real-time reverse transcription-polymerase chain reaction (RT-PCR)** has been employed in the current situation.

Computed Tomography (CT) as well as X-ray images play a significant role in the primary analysis of this infection and provide the treatment accordingly [32]. Because of minimum RT-PCR, sensitivity becomes limited, even while getting negative results, and symptoms are predicted by analyzing the radiological photographs of patients. It is assumed that CT is one of the sensitive models in detecting COVID-19 pneumonia, which acts as a screening device along with RT-PRC. Based on the study of lung CT, patients who are suffering from COVID-19 pneumonia should be observed for 10 days after the onset of symptoms. Next, Chinese clinical centers were projected with limited test devices, which resulted in a higher rate of false and negative results, thus physicians are forced to diagnose the disease according to medical as well as chest CT outcomes [8]. CT is one of the well-known scanning tools applied for the prediction of COVID-19 in many countries like Turkey, where limited test kits are available.

Several developers have stated that integration of medical image features along with lab results are useful for COVID-19 prediction [11, 13, 18, 20, 23, 25]. Few works have found the modifications in chest X-ray as well as CT images before initializing the symptoms of COVID-19 [10]. As an inclusion, **Machine Learning (ML)** models were applied for automated disease diagnosis in the healthcare field, which has gained maximum attention from many doctors and caretakers. Also, **Deep Learning (DL)**, is another well-known application in **Artificial Intelligence (AI)** that activates the development of dedicated methods for accomplishing best simulation outcome with the help of input data, with no requirement of manual feature extraction [3–6, 15, 19, 28].

DL methods are effectively employed for massive issues such as arrhythmia prediction, skin cancer categorization classification, breast cancer prediction, brain disease categorization, pneumonia prediction from chest X-ray images, fundus image segregation, as well as lung segregation. An increase of COVID-19 requires massive medical professionals and hospitals for effective treatment. It has improved the interest in deploying an automatic prediction model according to the AI schemes. Unfortunately, it is a complicated operation to offer reputed medical centers and physicians due to various factors like cost. Hence, simple, précise, and robust AI methods are highly applicable to resolve these issues and offer periodical assistance for patients.

Even though radiologists play an important role because of the wider knowledge in this application, AI models in radiology could help attain exact analysis [9]. In recent times, massive radiology photographs are extensively applied for COVD19 prediction. Hemdan et al. [14] applied DL methods for diagnosing COVID-19 from Xray images and projected a COVIDX-Net method with seven CNN technologies. Another deep framework called COVID-Net is presented in Reference [29] that has accomplished the best accuracy while classifying healthy, non-COVID pneumonia, as well as COVID-19 categories.

Ioannis et al. [7] depicted the DL method with the application of 224 positive COVID-19 images. As a result, this technique has obtained maximum success rates for 2 and 3 categories, correspondingly. Narin et al. [22] attained a higher COVID-19 prediction accuracy with the help of chest X-ray images in conjunction with the ResNet50 approach. Sethy and Behera [26] categorized the features attained from diverse CNN methods with the **Support Vector Machine (SVM)** classification model under the application of X-ray photographs. This study reveals that the ResNet50 method with the SVM classification model offered an optimized function. Consequently, various studies on COVID-19 prediction are applied for diverse DL methods with CT images.

This article develops a new **synergic DL (SDL)**-based COVID-19 classification model in Chest X-Ray images. Initially, the SDL model makes use of dual DCNNs and undergoes a mutual learning process to learn details from one another; particularly, the representation of images learned by both DCNNs, which are provided as input to the synergic network. To increase the performance of the SDL technique, the **fuzzy bilateral filtering (FBF)** technique is applied as a preprocessing step, which considerably helps to increase the classification outcome for COVID-19 diagnosis. A sequence of simulations takes place using benchmark Chest X-ray images to confirm the goodness of the SDL model.

2 THE PROPOSED SDL MODEL FOR COVID-19 DIAGNOSIS

The newly deployed SDL model involves different processes, as shown in Figure 1. The figure portrayed that the SDL model undergoes initial processing using the FBF technique to enhance the quality of chest X-ray images; followed by the feature extraction process, which is carried out on preprocessed images and extracts a useful set of feature vectors. Finally, the feature vectors are classified to determine the presence of COVID-19 or non-COVID 19.

2.1 FBF-based Preprocessing

Initially, the Chest X-ray images undergo preprocessing using the FBF technique for maximizing the image quality.

2.1.1 Overview of Bilateral Filtering (BF). Assume that F is a multi-channel image as well as consider W as a sliding window of definite size $n \times n$. Let, pixels in W implied in the Cartesian Coordinate points and implied by $i = (i_1, i_2) \in Y^2$ the location of a pixel F_i in W in which $Y = \{0, 1, \ldots, n-1\}$ is capable. Based on Reference [27], BF substitutes the middle pixels of the filtering window by a weighted average of corresponding nearby pixel values. Hence, the

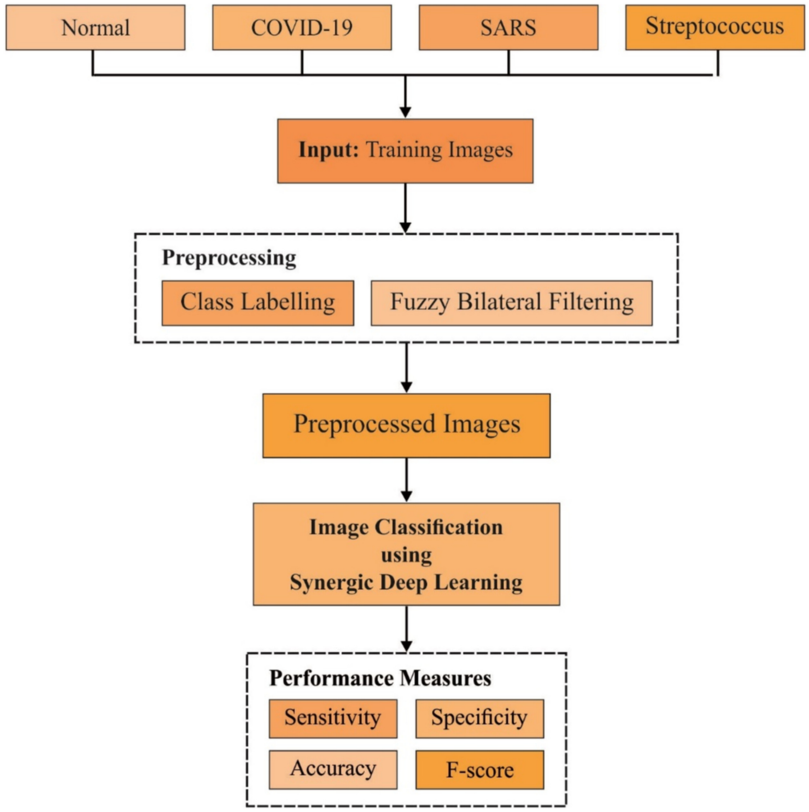

Fig. 1. Flowchart of proposed model.

weighting function was developed for smoothening the same colors at the time of retaining the edges unbroken by heavily weighted pixels that are spatially adjacent and the same in the middle pixel.

It is implied by $||\cdot||_2$ and Euclidean norm as well as by F_i is a central pixel. Next, weight $\mathcal{W}(F_i,\ F_j)$ for any pixel F_j in light to F_i is a combination of 2 units, namely, 1 spatial and 1 photometrical as given below:

$$\mathcal{W}(F_i,\ F_j) = \mathcal{W}_s(F_i,\ F_j)\mathcal{W}_p(F_i,\ F_j), \tag{1}$$

where spatial element $\mathcal{W}_s(F_i,\ F_j)$ is expressed as

$$\mathcal{W}_s(F_i,\ F_j) = e^{-\frac{||i-j||_2^2}{2\sigma_s^2}}. \tag{2}$$

Also, the photometrical element $\mathcal{W}_p(F_i,\ F_j)$ is represented as

$$-\frac{\Delta E_{Lab}(F_i, F_j)^2}{2\sigma_p^2}, \tag{3}$$

$$\mathcal{W}_p(F_i,\ F_j) = e, \tag{4}$$

where $\Delta E_{Lab} = [(\Delta L^*)^2 + (\Delta a^*)^2 + (\Delta b^*)^2]^{\frac{1}{2}}$ represents a perceptual color error from $L^*a^*b^*$ color space, and $\sigma_s, \sigma_p > 0$.

A color vector result F_i of a filter is processed by applying generalized weights and it is provided by

$$\widetilde{F_i} = \frac{\sum_{F_j \in \mathrm{W}} \mathcal{W}(F_i, F_j) F_j}{\sum_{F_j \in \mathrm{W}} \mathcal{W}(F_i, F_j)}. \tag{5}$$

The $\mathcal{W}_s$ weighting function is reduced while the spatial distance of an image from i and j is increased, and $\mathcal{W}_p$ weighting function is limited when perceptual color difference among the color vectors is enhanced.

The attributes σ_s and σ_p has been applied for modifying the influence of spatial as well as photometric elements, correspondingly. It is apparent that if σ_p?8, then BF models a Gaussian filter and if σ_s?8 a filter seeks for a range filter without spatial function. At this point, while σ_p?8 and σ_s?8 are existed, BF acts as an AMF.

2.1.2 Concept of Fuzzy Metric. Based on Reference [12], a fuzzy metric space is a $(X,\ M,\ *)$ in which X is a (nonempty) set, $*$ denotes a continuous t-norm and M implies a fuzzy set of $X \times X \times]O, +\infty$ for all $a, b, c \in X, s, t > 0$:

$(FM1) M(a,\ b,\ t) > 0$;

$(FM2) M(a,\ b,\ t) = 1$ if and only if $a = b$;

$(FM3) M(a,\ b,\ t) = M(b,\ a,\ t)$;

$(FM4)\ M\,(a,\ c,\ t + s) = M\,(a,\ b,\ t) * M\,(b,\ c,\ s)$;

$(FM5) M(a,\ b,\ \cdot)$:$]0, +\infty[[0, 1]$ is continuous.

$M(a,\ b,\ t)$ shows the degree of closeness for a and b by means of t. When $(X,\ M,\ *)$ is a fuzzy metric space, which is represented as $(M,\ *)$.

A fuzzy metric M on a is referred to as static while M is independent on t, where each $a, b \in X$ the function $M_{a,b}(t) = M(a,\ b,\ t)$ is named as constant. Hence, it is expressed as $M(a,\ b)$ by replacing $M(a,\ b,\ t)$.

Here, two fuzzy metrics have been applied. Initially, it is employed for estimating the photometric fuzzy distance among color vectors, while the latter one is used for measuring spatial fuzzy distance among pixels by comparing them. Hence, an accurate value can be obtained from photometric fuzzy distance from color vectors. Also, fuzzy metric M is applied:

Consider $X = \{0, 1, 2, \ldots, 255\}$ and let $K > 0$ is allocated. It is represented by $(F_i^1,\ F_i^2,\ F_i^3) \in X^3$ the color vector of a pixel F_i. The expression $M\ :\ X^3 \times X^3 ?]\ 0, 1]$ is described as:

$$M\left(F_i,\ F_j\right) = \prod_{s=1}^{3} \frac{\min\left\{F_i^s, F_j^s\right\}\ + K}{\max\left\{F_i^s, F_j^s\right\}\ + K}. \tag{6}$$

Based on Reference [21], a stationary fuzzy metric on X^3 has been attained. Existing operations have showcased that an adaptable measure of K attribute for reputed RGB images is $K = 1,024$, thus, the value is considered from the entire work. Also, $M(F_i, F_j)$ refers to a photometric fuzzy distance from color pixels F_i and F_j.

Then, the spatial fuzzy distance among pixels apply the definition in Section 2.1.1, which is indicated by $i = (i_1,\ i_2) \in Y^2$ the location of a pixel F_i in the window W. The expression $M_{||\cdot||_2}\ : Y^2 \times]\ 0,\ +8?]\ 0, 1]$ is provided, as

$$M_{||\cdot||_2}\,(i, j,\ t) = \frac{t}{t + ||i - j||_2} \tag{7}$$

is a fuzzy metric on Y^2 named as better fuzzy metric determined from Euclidean norm $||\cdot||_2$. In addition, $M_{||\cdot||_2}(i, j,\ t)$ refers to spatial fuzzy distance among color pixels F_i and F_j in terms of t. It is clear that $M_{||\cdot||_2}$ is autonomous for the length of Y; however, the relative position of an image

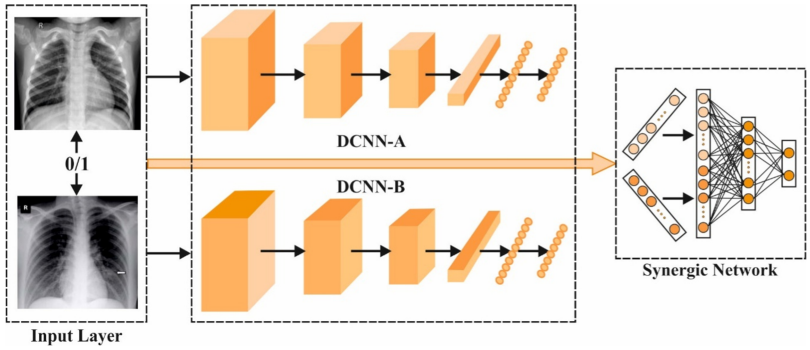

Fig. 2. Flowchart of SDL.

for pixels F_i and F_j has been compared. The t parameter is interpreted as a variable for changing the significance of spatial closeness criterion.

2.1.3 Fuzzy Bilateral Filtering. For defining the FBF method, it is essential to compute the weight of a pixel in a filtering window under the application of fuzzy metrics. As the pixel F_i is categorized by RGB color vector $(F_i^1,\ F_i^2,\ F_i^3)$ and by the position (i_1, i_2) in the window, it is assumed with a fuzzy metric of integrating $M(5)$ with $M_{||\cdot||_2}(6)$. Thus, to calculate the weights of a pixel $F_j, j \in W$ it considers the given function,

$$CFM(F_i,\ F_j,\ t) = M(F_i,\ F_j) \cdot M_{||\cdot||_2}(i, j,\ t) = \prod_{s=1}^{3} \frac{\min\left\{F_i^s, F_j^s\right\} + K}{\max\left\{F_i^s, F_j^s\right\} + K} \cdot \frac{t}{t + ||i - j||_2}. \tag{8}$$

While identifying pixel F with $(F_i^1,\ F_i^2,\ F_i^3,\ i_1,\ i_2)$, then the predefined function CFM is a fuzzy metric on $X^3 \times Y^2$. Likewise, the application of the previous fuzzy metric is sufficient for the concurrent method in spatial closeness as well as photometric similarity criteria. The FBF result is determined by

$$\widetilde{F_i} = \frac{\sum_{F_j \in \mathrm{W}} CFM(F_i, F_j, t) F_j}{\sum_{F_j \in \mathrm{W}} CFM(F_i, F_j, t)}, \tag{9}$$

where t parameter is applied for tuning the significance of spatial closeness in light of photometric criterion. It is evident that, as same as BF, if t?8, then the FBF schemes apply a range filter with no spatial function.

2.2 SDL-based Classification

The projected SDL method (see Figure 2) is composed of three classes, namely, input layer, dual DCNN elements (DCNN?A/B), as well as a synergic system. Initially, it consumes a pair of images as input. Every DCNN element facilitates the learning procedure autonomously for image depiction by supervising the class labels. The synergic network validates the input image pair that comes under a similar class that is categorized into three categories.

2.2.1 Input Layer. Unlike the classical DCNNs, the presented SDL method approves pair of images as input that has been selected randomly from the training set. Every image, along with the class label, which is fed into DCNN element, and pair of images are composed of a neighboring label that is induced into the synergic network.

2.2.2 Dual DCNN Components. Though DCNN structures are incorporated in the SDL method, a pre-trained residual network is combined with 50 learnable layers [31] for DCNN modules, because of tradeoff among the image classification function and count of parameters. For applying ResNet-50 in this application, the actual classification layer is replaced with the FC layer of 1,024 neurons, an FC layer of K neurons and softmax layer, and invoked the attributes of these layers by sampling a uniform distribution $U(-O.05, 0.05)$. It is applied with an image sequence $X = \{x_1,\ x_2,\ x_M\}$ and corresponding class label sequence $Y = \{y_1,\ y_2,\ y_M\}$ for fine-tuning DCNN element, which aspires to discover the collection of variables θ that reduces the cross-entropy loss:

$$l(\theta) = -\frac{1}{M}\left[\sum_{i=1}^{M}\sum_{j=1}^{K} 1\{y_i = j\}\, logp\,(y_i = j \mid x_i; \theta)\right]. \tag{10}$$

The attained parameter sets for DCNN-I as well as DCNN-J are implied by $\theta^{(I)}$ as well as $\theta^{(J)}$, correspondingly, that is not distributed among two DCNNs while performing the optimization.

2.2.3 Synergic Network. It is composed of embedding, FC, and output layers, as shown in Figure 2. It is defined as the resulting outcome of the penultimate FC layer in DCNN-I and DCNN-J while forwarding the deep feature from an image u_i, u_j, is showcased in the following:

$$f_i = \mathcal{F}\left(\theta^{(A)},\ u_i\right),\ f_j = \mathcal{F}\left(\theta^{(B)},\ u_j\right). \tag{11}$$

It is combined with deep features collected from the images are fed as the input of the synergic network, depicted by $f_{i\circ j}$, and described the desired result in which the synergic label for pair of images are denoted as,

$$y_S(x_i,\ x_j) = \begin{cases} 1\ if\ y_i = y_j, \\ 0\ if\ y_i \neq y_j. \end{cases} \tag{12}$$

To eliminate the unbalance data issues, it fixes the ratio of intra-class image pairs for every batch. It is applicable for observing the synergic signal by including alternate sigmoid layer and applying binary cross-entropy loss, as defined by

$$l^{(S)}\left(\theta^{(S)}\right) = y_S logp\left(y_S = 0 \,\middle|\, f_{i\circ j}; \theta^{(S)}\right) + (1 - y_S)\, logp\left(y_S = 1 \,\middle|\, f_{i\circ j}; \theta^{(S)}\right), \tag{13}$$

where $\theta^{(S)}$ denotes the attributes of a synergic network. While a DCNN makes an appropriate solution, the error made by alternate DCNN results in a synergic error that facilitates additional force for learning the discriminative implication.

2.2.4 Training and Testing. It has been employed with **Data Augmentation (DA)**, along with random rotation as well as horizontal and vertical flips for data training, which aims to maximize the dataset and eliminate the over-fitting of the presented method. It is implied that two image batches as $X_A = \{x_{A1},\ x_{A2},\ x_{AM}\}, X_B = \{x_{B1},\ x_{B2},\ x_{BM}\}$, corresponding classification labels into Y_A, Y_B, and synergic label as Y_S. Once the processing of DCNN is completed, two sets of deep features F_A^1 and F_B^1 have been attained. Next, it combined the corresponding pair of deep feature maps and reached $F_{A\circ B}^1 = \{f_{A1\circ B1},\ f_{A2\circ B2},\ f_{AM\circ BM}\}$, which has been employed as an input of a synergic network. The two classification losses $l^{(A)}(\theta^{(A)})$, $l^{(B)}(\theta^{(B)})$ and synergic loss $l^{(S)}(\theta^{(S)})$ are considered as cross-entropy loss, which is represented as:

$$\theta^{(A)}(t+1) = \theta^{(A)}(t) - \eta(t) \cdot \Delta^{(A)}, \tag{14}$$

$$\theta^{(B)}(t+1) = \theta^{(B)}(t) - \eta(t) \cdot \Delta^{(B)}, \tag{15}$$

$$\theta^{(S)}(t+1) = \theta^{(S)}(t) - \eta(t) \cdot \Delta^{(S)}, \tag{16}$$

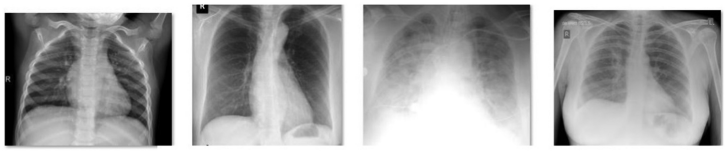

Fig. 3. Multi-Class (a) Normal (b) COVID-19 (c) SARS (d) Streptococcus.

Table 1. Binary Classification Results of FBF-SDL Model

No. of Runs	Sensitivity	Specificity	Accuracy	F-score
Run 1	96.10	96.06	96.05	96.21
Run 2	96.09	95.95	95.98	95.96
Run 3	96.23	96.30	96.25	96.13
Run 4	96.20	96.02	96.18	96.20
Run 5	95.90	96.22	96.19	96.18
Average	**96.10**	**96.11**	**96.13**	**96.14**

where $\Delta^{(A)} = \frac{\partial l^{(A)}(\theta^{(A)})}{\partial \theta(A)} + \lambda\Delta^{(S)}, \Delta^{(B)} = \frac{\partial l^{(B)}(\theta^{(B)})}{\partial \theta(B)} + \lambda\Delta^{(S)}, \Delta^{(S)} = \frac{\partial l^{(S)}(\theta^{(S)})}{\partial \theta(s)}$, λ denotes a subversion of classification error as well as synergic error, t indicates index of iteration, and $\eta(t) = \frac{\eta(0)}{1+10^{-4}\times t}$ refers to a variable learning measure with initialization $\eta(0) = 0.0001$.

In the testing stage, assume the probabilistic detection provided by DCNN components are described by $P^{(i)} = (p_1^{(i)}, p_2^{(i)}, \ldots, p_K^{(i)}), i = 1, 2$ as described in the following:

$$\underset{j}{argmax}\left\{\sum_{i=1}^{2} p_1^{(i)}, \ldots, \sum_{i=1}^{2} p_j^{(i)}, \ldots, \sum_{i=1}^{2} p_K^{(i)}\right\}. \tag{17}$$

3 EXPERIMENTAL VALIDATION

For experimentation, 10-fold cross-validation process is employed. The proposed model is implemented by the use of Intel i5, eighth generation PC with 16 GB RAM, MSI L370 Apro, Nividia 1050 Ti4 GB. For experimentation, Python 3.6.5 tool is used along with pandas, sklearn, Keras, Matplotlib, TensorFlow, opencv, Pillow, seaborn, and pycm. The parameter settings in the experimentation are given here: learning rate: 0.0001, momentum: 0.9, batch size: 128, and epoch count: 140. Some sample test images are illustrated in Figure 3.

3.1 Analysis of Binary Classification Results

Table 1 and Figure 4 perform a detailed investigation of the results attained by FBF-SDL model under binary classes with respect to different runs. The proposed FBF-SDL model has resulted in a higher classification outcome under all the applied runs. For instance, under the execution run of 1, the FBF-SDL model has resulted in a higher sensitivity of 96.10%, specificity of 96.06%, accuracy of 96.05%, and F-score of 96.21%. Likewise, under the execution run of 2, the FBF-SDL method has provided a maximum sensitivity of 96.09%, specificity of 95.95%, accuracy of 95.98%, and F-score of 95.96%. Additionally, under the execution run of 3, the FBF-SDL approach has accomplished a greater sensitivity of 96.23%, specificity of 96.30%, accuracy of 96.25%, and F-score of 96.13%. Simultaneously, under the execution run of 4, the FBF-SDL scheme has obtained a high sensitivity of 96.20%, specificity of 96.02%, accuracy of 96.18%, and F-score of 96.20%. In line with this, under

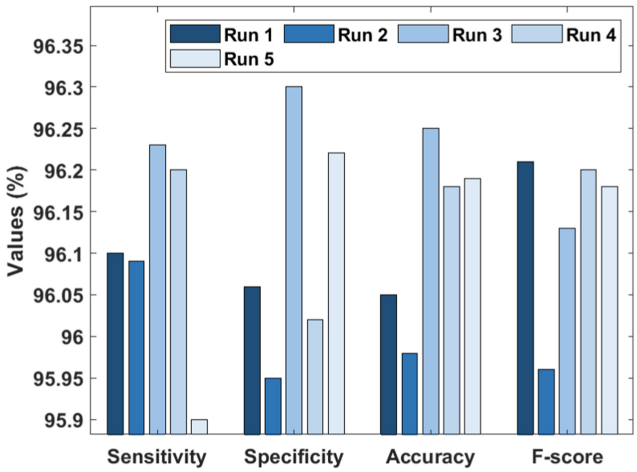

Fig. 4. Binary classification results of FBF-SDL model.

Table 2. Multi-classification Results of FBF-SDL Model

No. of Runs	Sensitivity	Specificity	Accuracy	F-score
Run 1	96.44	96.67	96.58	96.59
Run 2	96.10	96.23	96.21	96.19
Run 3	96.05	96.11	96.06	96.08
Run 4	96.21	95.90	96.18	95.92
Run 5	96.32	96.87	96.76	96.74
Average	**96.22**	**96.36**	**96.36**	**96.30**

the execution run of 5, the FBF-SDL framework has achieved a maximum sensitivity of 95.90%, specificity of 96.22%, accuracy of 96.19%, and F-score of 96.18%.

3.2 Analysis of Multi-classification Results

Table 2 and Figure 5 compute a brief examination of the simulation outcome achieved by the FBF-SDL method under Multi-class in terms of diverse runs. The newly developed FBF-SDL method has exhibited a high classification result under all the given runs.

For the sample, under the execution run of 1, the FBF-SDL approach has provided a greater accuracy of 96.58%, sensitivity of 96.44%. Along with that, under the execution run of 2, the FBF-SDL scheme has accomplished a better sensitivity of 96.10%, specificity of 96.23%, accuracy of 96.21%, and F-score of 96.19%. Furthermore, under the execution run of 3, the FBF-SDL scheme has achieved a maximum sensitivity of 96.05%, specificity of 96.11%, accuracy of 96.06%, and F-score of 96.08%. Meanwhile, under the execution run of 4, the FBF-SDL technology has attained a greater sensitivity of 96.21%, specificity of 95.90%, accuracy of 96.18%, and F-score of 95.92%. In the same way, under the execution run of 5, the FBF-SDL technology has achieved an optimal sensitivity of 96.32%, specificity of 96.87%, accuracy of 96.76%, and F-score of 96.74%.

Figure 6 shows the average analysis of the FBF-SDL model on Binary and Multi-classification in terms of different measures. The figure exhibited that binary class performed average result attained a sensitivity of 96.10%, specificity of 96.11%, accuracy of 96.13%, and F-score of 96.14%.

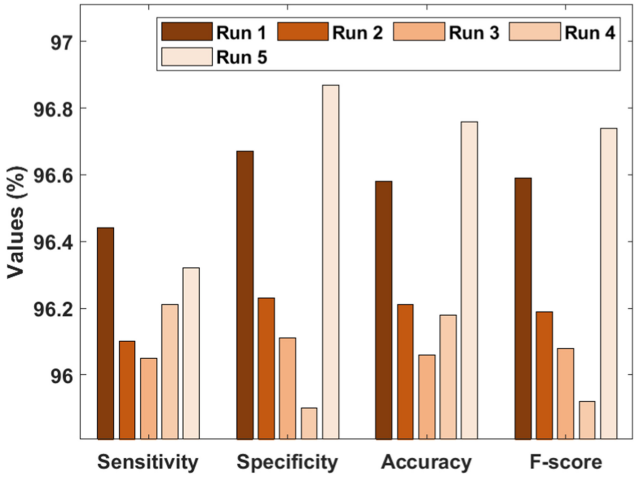

Fig. 5. Multi-classification results of FBF-SDL model.

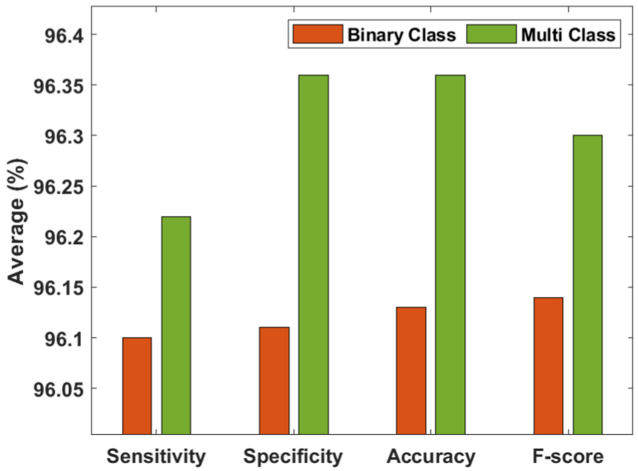

Fig. 6. Average analysis of binary and Multi-classification.

Likewise, the Multi-classes show that the higher average result obtained a sensitivity of 96.22%, specificity of 96.36%, accuracy of 96.36%, and F-score of 96.30%.

3.3 Comparative Results Analysis of FBF-SDL Model

Figure 7 performs a sensitivity analysis of the FBF-SDL model with recently presented models for COVID-19 classification. From the figure, it is evident that the DT and CNN models are found to be poor COVID-19 diagnosis performers, which have attained the sensitivity values of 87% and 87.73%. The ANFIS, KNN, and DTL models have outperformed the DT and CNN models with the closer sensitivity values of 88.48%, 89%, and 89.61%. In line with this, the CoroNet model has reached a moderate sensitivity of 90%. Simultaneously, the XGBoost, RNN, and CNNLSTM models have obtained slightly higher sensitivity values of 92%, 92.04%, and 92.14%. Concurrently, the MLP, LR, LSTM, and ANN models have tried to exhibit acceptable sensitivity values of 93%, 93%, 93.42%, and 93.78%, respectively. Furthermore, the CNNRNN model has led to a high sensitivity value of 94.23%.

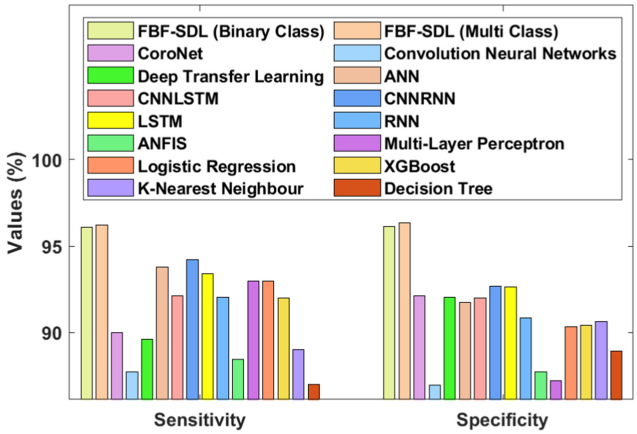

Fig. 7. Sensitivity and specificity analysis of FBF-SDL model.

But the proposed FBF-SDL models have attained a maximum sensitivity of 96.1% and 96.22% on binary and multi-classification, respectively.

The figure shows the specificity analysis of the FBF-SDL method with currently projected methods for COVID-19 categorization. From the figure, it is clear that the CNN and MLP methodologies are considered as inferior COVID-19 diagnosis performers, which has accomplished the specificity values of 86.97% and 87.23%. Then, the ANFIS, DT, and LR methods have surpassed the CNN and MLP approaches with identical specificity values of 87.74%, 88.93%, and 90.34%. Similarly, the XGBoost method has achieved a considerable specificity of 90.44%. At the same time, the KNN, RNN, and ANN methodologies have accomplished moderate specificity values of 90.65%, 90.87%, and 91.76%. Simultaneously, the CNNLSTM, DTL, CoroNet, and LSTM technologies have attempted to represent reasonable specificity values of 91.98%, 92.03%, 92.14%, and 92.64% correspondingly. Moreover, the CNNRNN approach has resulted in a higher specificity value of 92.67%. However, the projected FBF-SDL methods have reached a greater specificity of 96.11% and 96.36% on binary and multi-classification, respectively.

Figure 8 computes the accuracy analysis of the FBF-SDL method with currently projected technologies for COVID-19 classification. From the figure, it is apparent that the CNNLSTM and RNN schemes are said to be worse COVID-19 diagnosis performers that have achieved the same accuracy value of 84.16%. Then, the CNNRNN, ANN, and LSTM technologies have performed better than CNNLSTM and RNN methods with closer accuracy values of 85.66%, 86%, and 86.66%. Likewise, the DT approach has obtained a considerable accuracy of 86.71%. At the same time, CNN, MLP, and KNN schemes have attained moderate accuracy values of 87.36%, 88.11%, and 88.91%. Simultaneously, the CoroNet, DTL, XGBoost, and LR methods have attempted to display acceptable accuracy values of 90.21%, 90.75%, 91.57%, and 92.12% correspondingly. In addition, the MLP method has resulted in a maximum accuracy value of 93.13%. Thus, the presented FBF-SDL approaches have achieved a high accuracy of 96.13% and 96.36% on binary and multi-classification, respectively.

The figure determines an F-score analysis of the FBF-SDL method with presently developed methods for COVID-19 categorization. From the figure, it is portrayed that the DT and KNN schemes are referred to as ineffective COVID-19 diagnosis performers that have accomplished the F-score values of 87% and 89%. Then, the ANFIS, CNN, and CNNLSTM methodologies have surpassed the DT and KNN methods with the closer F-score values of 89.04%, 89.65%, and 90.01%.

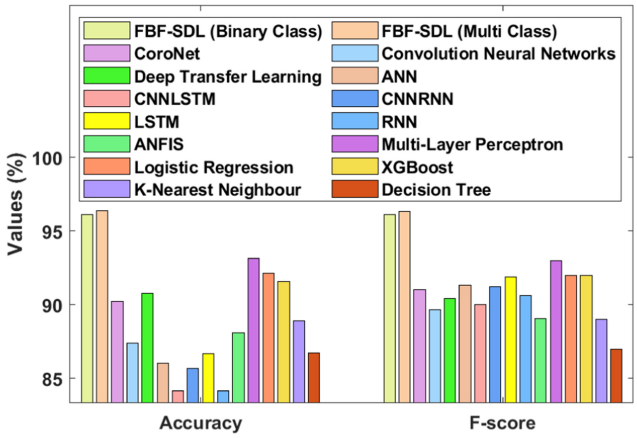

Fig. 8. Accuracy and F-score analysis of FBF-SDL model.

Similarly, the DTL approach has attained a considerable F-score of 90.43%. Concurrently, the RNN, CoroNet, and CNNRNN approaches have reached better F-score values of 90.61%, 91%, and 91.20%. Along with that, the ANN, LSTM, LR, and XGBoost frameworks have attempted to represent considerable F-score values of 91.34%, 91.89%, 92%, and 92%, respectively. In addition, the MLP technology has resulted in a maximum F-score value of 93%. Therefore, the projected FBF-SDL method has accomplished a higher F-score of 96.14% and 96.30% on binary as well as multi-classification, respectively.

4 CONCLUSION

This article has developed a new synergic DL based COVID-19 classification model in Chest X-Ray images. The SDL model undergoes initial processing using the FBF technique to improve the quality of the chest X-ray images. The feature extraction process is carried out on preprocessed images and extract a useful set of feature vectors. Finally, the feature vectors are classified to determine the presence of COVID-19 or non-COVID 19. The integration of FBL and SDL resulted in the effective classification of COVID-19. A detailed set of experimentations was carried out and the results are examined under distinct aspects. The experimental outcome demonstrated that the SDL model has appeared as an effective tool to classify the COVID-19 and non-COVID 19 patients using Chest X-ray images.

ACKNOWLEDGMENTS

Dr. K. Shankar and Dr. Eswaran Perumal would like to thank RUSA PHASE 2.0, Alagappa University, Karaikudi.

REFERENCES

[1] Yassine Abdulsalam and M. Shamim Hossain. 2020. COVID-19 networking demand: An auction-based mechanism for automated selection of edge computing services. *IEEE Trans. Netw. Sci. Eng.* (2020).

[2] Eman M. Abou-Nassar, Abdullah M. Iliyasu, Passent M. El-Kafrawy, Oh-Young Song, Ali Kashif Bashir, and Ahmed A. Abd El-Latif. 2020. DITrust chain: Towards blockchain-based trust models for sustainable healthcare IoT systems. *IEEE Access* 8 (2020), 111223–111238.

[3] Ahmed Alghamdi, Mohamed Hammad, Hassan Ugail, Asmaa Abdel-Raheem, Khan Muhammad, Hany S. Khalifa, and Ahmed A. Abd El-Latif. 2020. Detection of myocardial infarction based on novel deep transfer learning methods for urban healthcare in smart cities. *Multim. Tools Applic.* (2020), 1–22.

[4] Ahmed S. Alghamdi, Kemal Polat, Abdullah Alghoson, Abdulrahman A. Alshdadi, and Ahmed A. Abd El-Latif. 2020. Gaussian process regression (GPR) based non-invasive continuous blood pressure prediction method from cuff oscillometric signals. *Appl. Acoust.* 164 (2020), 107256.

[5] Ahmed S. Alghamdi, Kemal Polat, Abdullah Alghoson, Abdulrahman A. Alshdadi, and Ahmed A. Abd El-Latif. 2020. A novel blood pressure estimation method based on the classification of oscillometric waveforms using machine-learning methods. *Appl. Acoust.* 164 (2020), 107279.

[6] Mohammad A. Alsmirat, Fatimah Al-Alem, Mahmoud Al-Ayyoub, Yaser Jararweh, and Brij Gupta. 2019. Impact of digital fingerprint image quality on the fingerprint recognition accuracy. *Multim. Tools Applic.* 78, 3 (2019), 3649–3688.

[7] Ioannis D. Apostolopoulos and Tzani A. Mpesiana. 2020. Covid-19: Automatic detection from x-ray images utilizing transfer learning with convolutional neural networks. *Phys. Eng. Sci. Med.* (2020), 1.

[8] Adam Bernheim, Xueyan Mei, Mingqian Huang, Yang Yang, Zahi A. Fayad, Ning Zhang, Kaiyue Diao, Bin Lin, Xiqi Zhu, Kunwei Li, Shaolin Li, Hong Shan, Adam Jacobi, and Michael Chung. 2020. Chest CT findings in coronavirus disease-19 (COVID-19): Relationship to duration of infection. *Radiology* 295, 3 (June 2020), 200463. DOI: https://doi.org/10.1148/radiol.2020200463

[9] Federico Caobelli. 2020. Artificial intelligence in medical imaging: Game over for radiologists? *Eur. J. Radiol.* 126 (May 2020), 108940. DOI: https://doi.org/10.1016/j.ejrad.2020.108940

[10] Jasper Fuk-Woo Chan, Shuofeng Yuan, Kin-Hang Kok, Kelvin Kai-Wang To, Hin Chu, Jin Yang, Fanfan Xing, Jieling Liu, Cyril Chik-Yan Yip, Rosana Wing-Shan Poon, Hoi-Wah Tsoi, Simon Kam-Fai Lo, Kwok-Hung Chan, Vincent Kwok-Man Poon, Wan-Mui Chan, Jonathan Daniel Ip, Jian-Piao Cai, Vincent Chi-Chung Cheng, Honglin Chen, Christopher Kim-Ming Hui, and Kwok-Yung Yuen. 2020. A familial cluster of pneumonia associated with the 2019 novel coronavirus indicating person-to-person transmission: A study of a family cluster. *Lancet* 395, 10223 (Feb. 2020), 514–523. DOI: https://doi.org/10.1016/s0140-6736(20)30154-9

[11] K. DeviPriya and Sumalatha Lingamgunta. 2020. Multi factor two-way hash-based authentication in cloud computing. *Int. J. Cloud Applic. Comput.* 10, 2 (2020), 56–76.

[12] A. George and P. Veeramani. 1994. On some results in fuzzy metric spaces. *Fuzzy Sets Syst.* 64, 3 (June 1994), 395–399. DOI: https://doi.org/10.1016/0165-0114(94)90162-7

[13] Mohamed Hammad, Monagi H. Alkinani, B. B. Gupta, and Ahmed A. Abd El-Latif. 2021. Myocardial infarction detection based on deep neural network on imbalanced data. *Multim. Syst.* (2021), 1–13.

[14] Ezz El-Din Hemdan, Marwa A. Shouman, and Mohamed Esmail Karar. 2020. COVIDX-Net: A framework of deep learning classifiers to diagnose Covid-19 in X-ray images. *arXiv preprint arXiv:2003.11055* (2020).

[15] M. Shamim Hossain. 2015. Cloud-supported cyber–physical localization framework for patients monitoring. *IEEE Syst. J.* 11, 1 (2015), 118–127.

[16] M. Shamim Hossain, Ghulam Muhammad, and Nadra Guizani. 2020. Explainable AI and mass surveillance system-based healthcare framework to combat COVID-19 like pandemics. *IEEE Netw* 34, 4 (2020), 126–132.

[17] Srinidhi Jha, Manish Kumar Goyal, Brij Gupta, and Anil Kumar Gupta. 2021. A novel analysis of COVID-19 risk in India incorporating climatic and socio-economic factors. *Technol. Forecast. Soc. Change* (2021), 120679.

[18] Weifang Kong and Prachi P. Agarwal. 2020. Chest imaging appearance of COVID-19 infection. *Radiol.: Cardiothor. Imag.* 2, 1 (Jan. 2020), e200028. DOI: https://doi.org/10.1148/ryct.2020200028

[19] Yann LeCun, Yoshua Bengio, and Geoffrey Hinton. 2015. Deep learning. *Nature* 521, 7553 (May 2015), 436–444. DOI: https://doi.org/10.1038/nature14539

[20] Mehedi Masud, Gurjot Singh Gaba, Salman Alqahtani, Ghulam Muhammad, B. B. Gupta, Pardeep Kumar, and Ahmed Ghoneim. 2020. A lightweight and robust secure key establishment protocol for internet of medical things in COVID-19 patients care. *IEEE Internet Things J.* (2020).

[21] Samuel Morillas, Valentín Gregori, Guillermo Peris-Fajarnés, and Pedro Latorre. 2005. A new vector median filter based on fuzzy metrics. In *Lecture Notes in Computer Science*. Springer Berlin, 81–90. DOI: https://doi.org/10.1007/11559573_11

[22] Ali Narin, Ceren Kaya, and Ziynet Pamuk. 2020. Automatic detection of coronavirus disease (COVID-19) using x-ray images and deep convolutional neural networks. *arXiv preprint arXiv:2003.10849* (2020).

[23] Abdelwahhab Satta and Sihem Mostefai. 2020. Strategic outsourcing to cloud computing: A comprehensive framework based on analytic hierarchy process. *Int. J. Cloud Applic. Comput.* 10, 1 (2020), 11–27.

[24] Ahmed Sedik, Mohamed Hammad, Fathi E. Abd El-Samie, Brij B. Gupta, and Ahmed A. Abd El-Latif. 2021. Efficient deep learning approach for augmented detection of Coronavirus disease. *Neural Comput. Applic.* (2021), 1–18.

[25] Ahmed Sedik, Abdullah M. Iliyasu, Abd El-Rahiem, Mohammed E. Abdel Samea, Asmaa Abdel-Raheem, Mohamed Hammad, Jialiang Peng, Abd El-Samie, E. Fathi, Ahmed A. Abd El-Latif et al. 2020. Deploying machine and deep learning models for efficient data-augmented detection of COVID-19 infections. *Viruses* 12, 7 (2020), 769.

[26] Prabira Kumar Sethy and Santi Kumari Behera. 2020. Detection of coronavirus disease (COVID-19) based on deep features. (Mar. 2020). Preprints 2020.

[27] C. Tomasi and R. Manduchi. 1998. Bilateral filtering for gray and color images. In *6th International Conference on Computer Vision (IEEE Cat. No.98CH36271)*. Narosa Publishing House. https://doi.org/10.1109/iccv.1998.710815

[28] Haoxiang Wang, Zhihui Li, Yang Li, B. B. Gupta, and Chang Choi. 2020. Visual saliency guided complex image retrieval. *Pattern Recog. Lett.* 130 (2020), 64–72.

[29] Linda Wang and Alexander Wong. 2020. COVID-Net: A tailored deep convolutional neural network design for detection of COVID-19 cases from chest X-Ray images. *arXiv preprint arXiv:2003.09871* (2020).

[30] Fan Wu, Su Zhao, Bin Yu, Yan-Mei Chen, Wen Wang, Zhi-Gang Song, Yi Hu, Zhao-Wu Tao, Jun-Hua Tian, Yuan-Yuan Pei, Ming-Li Yuan, Yu-Ling Zhang, Fa-Hui Dai, Yi Liu, Qi-Min Wang, Jiao-Jiao Zheng, Lin Xu, Edward C. Holmes, and Yong-Zhen Zhang. 2020. A new coronavirus associated with human respiratory disease in China. *Nature* 579, 7798 (Feb. 2020), 265–269. DOI: https://doi.org/10.1038/s41586-020-2008-3

[31] Jianpeng Zhang, Yutong Xie, Qi Wu, and Yong Xia. 2018. Skin lesion classification in dermoscopy images using synergic deep learning. In *Medical Image Computing and Computer Assisted Intervention – MICCAI 2018*. Springer International Publishing, 12–20. DOI: https://doi.org/10.1007/978-3-030-00934-2_2

[32] Zi Yue Zu, Meng Di Jiang, Peng Peng Xu, Wen Chen, Qian Qian Ni, Guang Ming Lu, and Long Jiang Zhang. 2020. Coronavirus disease 2019 (COVID-19): A perspective from China. *Radiology* 296, 2 (Aug. 2020), E15–E25. DOI: https://doi.org/10.1148/radiol.2020200490

Received September 2020; revised November 2020; accepted February 2021